Valley-polarized beam propagation in metallic photonic graphene

Kang Wang
Université Paris-Saclay, CNRS, Laboratoire de Physique des Solides, 91405, Orsay, France
e-mail: kang.wang@u-psud.fr

ABSTRACT

We investigate the electromagnetic wave propagation in a triangular metallic photonic graphene structure and show that, associated to trigonally warped Dirac cones, the transport properties resulting from an incident beam at the armchair edge display drastically different behaviors as compared to the results obtained for other analogous systems. Namely, associated to the lower Dirac cone, the incident beam is collimated to one center beam; while, associated to the upper cone, it is split into two beams with a $2\pi/3$ angle. The other expected beams are all strongly inhibited. This can be related to the metallic nature of the structure, where a propagating electromagnetic wave should follow the structure locals patterns that govern its field distribution, whose symmetry properties determine its excitation by an incident wave. This study highlights the singularity of a metallic photonic graphene in its interaction with the electromagnetic waves, and may find applications in valley photonics for high efficiency collimating and large angle beam splitting system designs.

Keywords: metallic photonic graphene, Dirac cone, transport, valley photonics.

INTRODUCTION

Graphene-like photonic structures provide opportunities for optically probing Dirac cone related physical properties and attract enormous interest. Potential applications, such as valley photonics exploring optically the valley degree of freedom associated to Dirac cones[1], analogous to valleytronics [2], have recently been proposed for information processing [3]. Indeed, it is known that, in a honeycomb structure, the Dirac cones undergo trigonal warping departing from the Dirac level [4]. When their iso-frequency contours become nearly triangular, beam splitting and self-collimation associated to different K points occur due to the anisotropic group velocity distribution [1], offering possibilities for wave propagation control and beam manipulation. Studies on valley-polarized EM wave propagation in photonic graphenes are limited to dielectric structures [1], [5]. These studies concern, moreover, only the lower Dirac cones. Concerning the upper cones, there are reports on analogous situations of electron beam propagation in mono- and bi-layer graphenes [6], [7].

Regarding the metallic photonic structures, Dirac cones are obtained for triangular structures [8], [9], where the low-frequency electromagnetic (EM) bands are formed by cavity-like EM resonance modes formed inside the triangular structural units. The band structure can be described by a tight binding (TB) model, with the crystal eigenmodes as superpositions of these local modes [9]. As a consequence, EM wave propagation in such structures is realized through the coupling between the structural units, and will be determined by the structure local patterns by following the structural unit distribution. We investigate in the present work the propagation of EM waves associated to the Dirac cones from the armchair edge in a triangular metallic photonic graphene structure. We show that, compared to the studies mentioned above [1], [5], [6], the beam propagation in such a photonic structure displays drastically different behaviors.

ELECTROMAGNETIC BEAM PROPAGATION

A triangular lattice [Fig. 1(a)] contains two families (A and B) of triangular structural units. The metallic structure is constructed by infinite cylinders, with radius $r = 0.25a$ (a being the lattice constant) and dielectric constant set to negative infinity, placed at the lattice nodes in an air background. The EM frequency band diagram for TM polarization (the electric field parallel to z axis), obtained by solving Maxwell's equations using the finite-difference time-domain (FDTD) method, is displayed in Fig. 1(b). Dirac cones are formed by the first two bands, of which a 3D view at K ($4\pi/3a$, 0) point is shown in Fig. 1(c). The iso-frequency contours of the upper and lower Dirac cones are depicted in the same figure [1(d) and 1(e)]. The iso-frequency lines take quasi-triangular forms at $\omega_1 \approx 0.863$ and $\omega_2 \approx 0.978$ ($\omega a/2\pi c$) for respectively the lower and the upper cones.

In a TB model [9], the crystal wave function along Γ-K direction is expressed as

$$|\Psi_{\mathbf{k}}(\mathbf{r})\rangle = \sum_m \frac{e^{i\mathbf{k}\mathbf{R}_m}}{\sqrt{2N}} (|\phi_A(\mathbf{r} - \mathbf{R}_m - \mathbf{d}_A)\rangle \pm |\phi_B(\mathbf{r} - \mathbf{R}_m - \mathbf{d}_B)\rangle) \quad (1)$$

with $|\phi_A\rangle$ and $|\phi_B\rangle$ corresponding respectively to the electric field distributions of the resonance modes formed inside A and B triangles. The wave function is characterized by a mirror or a mirror inversion symmetry with respect to the plane defined by the Γ-K line and the z axis, determined by the $\pm$ signs, and can be described by

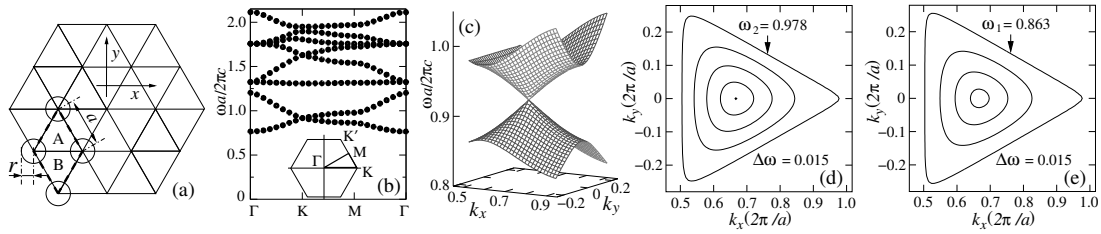

Figure 1. Triangular photonic structure (a) and the corresponding EM frequency band diagram (b). A 3D view of the Dirac cone at K $(4\pi/3a,\ 0)$, formed by the first two bands, is shown in (c). Iso-frequency contours of the upper and lower cone at the same K point are depicted in (d) and (e), where the frequency level (ω_1 and ω_2) as well as the contour interval ($\Delta\omega$) values are normalized to $\omega a/2\pi c$.

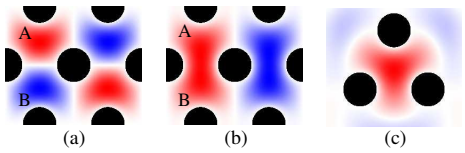

Figure 2. Electric field distributions corresponding to the upper (a) and lower (b) Dirac band branch at $k = (\pi/a, 0)$, and in an individual triangle (c).

the A_1 and B_1 representations of the C_{2v} group [10]. This symmetry relation can further be checked by the field distributions. As an example, the electric field distributions of the two band branches at $k = (\pi/a, 0)$, together with that in an individual triangle, obtained by the FDTD method, are displayed in Fig. 2, which shows that, for the lower or upper band, the electric fields in the A and B triangles display the same or opposite polarities.

This will impact directly the wave propagation for an incident beam along the Γ-K direction, where self-collimation effects are obtained for EM waves and electron beams in respectively dielectric photonic and atomic graphenes, with, perpendicular to the iso-frequency contours, one self-collimated center beam along the incident direction and two side beams along the $\pm\pi/3$ directions, associated to the lower or upper Dirac cones [1], [5], [6]. In the present case, a center beam described by the A_1 representation can be coupled to a TM polarized incident beam along the Γ-K direction, while there can not be coupling for a center beam described by the B_1 representation, the incident beam being characterized by a mirror symmetry plane defined by the Γ-K line and the z axis. Similarly, the coupling with the side beams will also be determined by their symmetry relations with the field patterns associated to the incident beam at the sample edge.

Let us consider a sample containing 18x15 periods [Fig. 3(a) and (b)]. The TM polarized beams are injected on the armchair edge through a metallic wave guide of width $4a$. Two monochromatic waves, corresponding to the lower ($\omega_1 = 0.863$) and upper ($\omega_2 = 0.978$) nearly triangular iso-frequency contour levels of the Dirac cones, are considered. The wave propagation in the sample is obtained using the FDTD method. It is obvious that, compared to the lower part insets, at ω_1, the expected side beams associated to the K′ point are almost absent, and only the center beam associated to K and K′ points displays significant amplitude; while, at ω_2, the expected center beam associated to K and K′ points is almost absent, and only the two side beams associated to the K point display significant amplitude.

For a more quantitative description, we consider the transmission spectra, normalized by the incident flux, in two out-going regions with the same width as the incident wave guide. One is placed across the sample in front of the incident beam (center beam direction); the other is placed on the sample upper side at $\pi/3$ angle (side beam direction). The transmission spectra obtained by the FDTD method, centered at Dirac frequency ω_D, are displayed in Fig. 3(c), with the transmission spectrum in the side beam direction multiplied by 2. Figure 3(c) shows that, in the center beam direction, the transmission associated to the lower cone is predominant, and reaches its maximum near ω_1; while, in the side beam directions, the transmission associated to the upper cone is predominant, and reaches its maximum near ω_2. The transmissions in the side beam directions associated to the lower cone and in the center beam direction associated to the upper cone are much weaker. Their maxima, around ω_1 and ω_2, are one order of magnitude lower than their counterparts. This corroborates the field distributions in Fig. 3(a) and (b).

As mentioned above, these particular behaviors are to be linked to the symmetries of both the incident beam and the frequency bands. Figure 3 shows that the field distribution of the center beam at ω_1 can be described by the A_1 representation, with a mirror symmetry with respect to the xz plane; while, at ω_2, the field distribution of each of the side beams can be described by the B_1 representation, with a mirror inversion symmetry with respect to the plane defined by the z axis and the propagation direction. This is in agreement with the band symmetry discussed above. Moreover, the symmetries of these propagating beams are compatible with that of the incident beam and can be coupled to the latter. On the contrary, the center beam at ω_2, that should also belong to the B_1 representation, can not be coupled to the incident beam. Concerning the two side beams associated to the lower cone, considering a unit cell at the sample edge at the beginning of the paths in the $\pi/3$

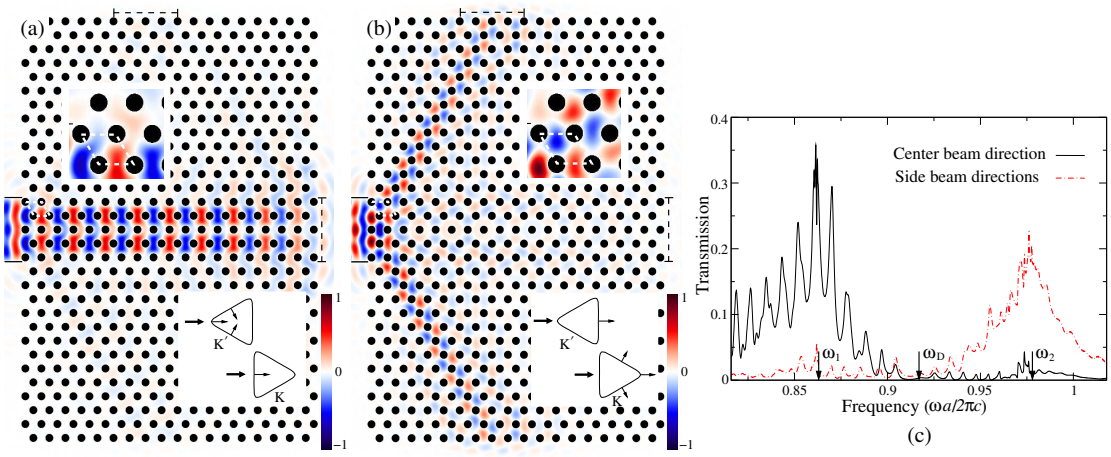

Figure 3. Electric field distributions of two monochromatic waves of frequencies ω_1 (a) and ω_2 (b), propagating in a 18x15 period sample. The incident beam is injected through a wave guide at the left side. The insets in the lower parts indicate the incident (thick arrows) and expected propagation (thin arrows) directions. The insets in the upper parts display a magnified zone around the unit cell in the incident region. The dashed lines indicate the out-going regions where the wave transmissions (c) are considered.

direction [the upper part inset in Fig. 3(a)], the local electric fields in the two triangles forming the unit cell are of opposite polarities. The coupling with an A_1 beam propagating along the $\pi/3$ direction is destructive. This accounts for the strong inhibition of the side beams at ω_1. In comparison, the local electric field in the same triangles, associated to the upper cone [the upper part inset in Fig. 3(b)], can be constructively coupled with a B_1 beam propagating in the same direction. This explains the side beam excitation at ω_2.

CONCLUDING REMARKS

The EM wave propagation in a triangular metallic photonic graphene structure displays drastically different behaviors as compared to other analogous systems. Such a structure allows, on one hand, a better beam self-collimation associated to the lower Dirac cone, the side beams at the K′ point being almost absent, and, on the other hand, associated to the upper cone, it enables beam splitting at one Dirac point by allowing two strong side beams and inhibiting the center one, with the exclusion of the other Dirac point, allowing addressing directly and separately each Dirac point, and obtaining the response from a selected single Dirac point. It may find application in valley photonics in the designs of high efficiency beam collimators to convey information associated to both two valleys, and large angle splitters for the beam carrying information associated to a single specific valley.

REFERENCES

[1] J. L. Garcia-Pomar, A. Cortijo, and M. Nieto-Vesperinas, "Fully valley-polarized electron beams in graphene," Phys. Rev. Lett., vol. 100, 236801, June 2008

[2] A. Rycerz, J. Tworzydlo, and C. W. J. Beenakker, "Valley filter and valley valve in graphene," Nat. Phys., vol. 3, pp. 172-175, March 2007

[3] J.-W. Dong, X.-D. Chen, H. Zhu, Y. Wang, and X. Zhang, "Valley photonic crystals for control of spin and topology," Nat. Mater., vol. 16, pp. 298-302, March 2017

[4] R. Saito, G. Dresselhaus, and M. S. Dresselhaus, "Trigonal warping effect of carbon nanotubes," Phys. Rev. B, vol. 61, pp. 2981-2990, Jan. 2000

[5] F. Deng, et al., "Observation of valley-dependent beams in photonic graphene," Opt. Express, vol. 22, pp. 23605-23613, Sept. 2014

[6] Z. Wang and F. Liu, "Manipulation of electron beam propagation by hetero-dimensional graphene junctions," ACS Nano, vol. 4, pp. 2459-2465, April 2010

[7] C. Park, "Generation of valley-polarized electron beam in bilayer graphene," J. of Appl. Phys., vol. 118, 244301, Dec. 2015

[8] S. Bittner, et al., "Observation of a Dirac point in microwave experiments with a photonic crystal modeling graphene," Phys. Rev. B, vol. 82, 014301, July 2010

[9] K. Wang, "Low-frequency photonic band structures in graphene-like triangular metallic lattice," Mater. Res. Express, vol. 3, 115007, Nov. 2016

[10] See, for example, J. R. Ferraro, and K. Nakamoto, Introductory Raman Spectroscopy, 1st ed., San Diego, CA: Academic Press, 1994, p. 337